Chapter 23

Deterministic diffusion

This is a bizzare and discordant situation.
M.V. Berry

(R. Artuso and P. Cvitanović)

The advances in the theory of dynamical systems have brought a new life to Boltzmann's mechanical formulation of statistical mechanics. Sinai, Ruelle and Bowen (SRB) have generalized Boltzmann's notion of ergodicity for a constant energy surface for a Hamiltonian system in equilibrium to dissipative systems in nonequilibrium stationary states. In this more general setting the attractor plays the role of a constant energy surface, and the SRB measure of sect. 9.1 is a generalization of the Liouville measure. Such measures are purely microscopic and indifferent to whether the system is at equilibrium, close to equilibrium or far from it. "Far for equilibrium" in this context refers to systems with large deviations from Maxwell's equilibrium velocity distribution. Furthermore, the theory of dynamical systems has yielded new sets of microscopic dynamics formulas for macroscopic observables such as diffusion constants and the pressure, to which we turn now.

We shall apply cycle expansions to the analysis of *transport* properties of chaotic systems.

The resulting formulas are exact; no probabilistic assumptions are made, and the all correlations are taken into account by the inclusion of cycles of all periods. The infinite extent systems for which the periodic orbit theory yields formulas for diffusion and other transport coefficients are spatially periodic, the global phase space being tiled with copies of a elementary cell. The motivation are physical problems such as beam defocusing in particle accelerators or chaotic behavior of passive tracers in 2-d rotating flows, problems which can be described as deterministic diffusion in periodic arrays.

In sect. 23.1 we derive the formulas for diffusion coefficients in a simple physical setting, the 2-d periodic Lorentz gas. This system, however, is

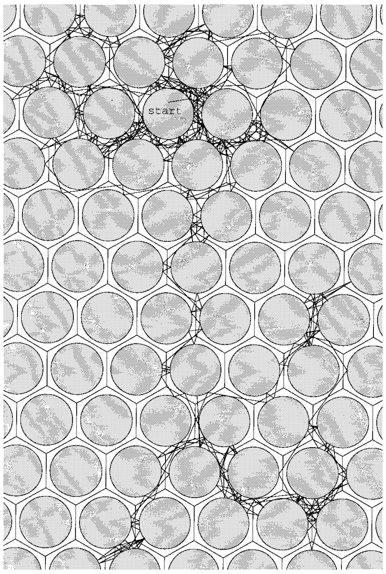

Figure 23.1: Deterministic diffusion in a finite horizon periodic Lorentz gas. (Courtesy of T. Schreiber)

not the best one to exemplify the theory, due to its complicated symbolic dynamics. Therefore we apply the theory first to diffusion induced by a 1-d maps in sect. 23.2and return to the Lorentz systems in sect. 23.4, after a brief disscusion of anomalous diffusion in sect. 23.3.

⇓PRIVATE
⇑PRIVATE

23.1 Diffusion in periodic arrays

The 2-d *Lorentz gas* is an infinite scatterer array in which diffusion of a light molecule in a gas of heavy scatterers is modelled by the motion of a point particle in a plane bouncing off an array of reflecting disks. The Lorentz gas is called "gas" as one can equivalently think of it as consisting of any number of pointlike fast "light molecules" interacting only with the stationary "heavy molecules" and not among themselves. As the scatterer array is built up from only defocusing concave surfaces, it is a pure hyperbolic system, and one of the simplest nontrivial dynamical systems that exhibits deterministic diffusion, figure 23.1. We shall now show that the *periodic* Lorentz gas is amenable to a purely deterministic treatment. In this class of open dynamical systems quantities characterizing global dynamics, such as the Lyapunov exponent, pressure and diffusion constant, can be computed from the dynamics restricted to the elementary cell. The method applies to any hyperbolic dynamical system that is a periodic tiling $\hat{\mathcal{M}} = \bigcup_{\hat{n}\in T} \mathcal{M}_{\hat{n}}$ of the dynamical phase space $\hat{\mathcal{M}}$ by *translates* $\mathcal{M}_{\hat{n}}$ of an *elementary cell* $\mathcal{M}$, with T the Abelian group of lattice translations. If the scattering array has further discrete symmetries, such as reflection symmetry, each elementary cell may be built from a *fundamental domain* $\widetilde{\mathcal{M}}$ by the action of a discrete (not necessarily Abelian) group G. The symbol $\hat{\mathcal{M}}$ refers here to the full phase space, that is,, both the spatial coordinates and the momenta. The spatial component of $\hat{\mathcal{M}}$ is the complement of the disks in the *whole* space.

We shall now relate the dynamics in $\mathcal{M}$ to diffusive properties of the Lorentz gas in $\hat{\mathcal{M}}$.

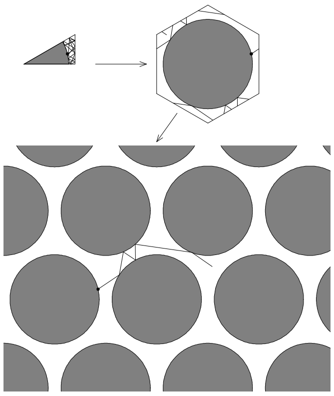

Figure 23.2: Tiling of $\hat{\mathcal{M}}$, a periodic lattice of reflecting disks, by the fundamental domain $\widetilde{\mathcal{M}}$. Indicated is an example of a global trajectory $\hat{x}(t)$ together with the corresponding elementary cell trajectory $x(t)$ and the fundamental domain trajectory $\tilde{x}(t)$. (Courtesy of J.-P. Eckmann)

These concepts are best illustrated by a specific example, a Lorentz gas based on the hexagonal lattice Sinai billiard of figure 23.2. We distinguish two types of diffusive behavior; the *infinite horizon* case, which allows for infinite length flights, and the *finite horizon* case, where any free particle trajectory must hit a disk in finite time. In this chapter we shall restrict our consideration to the finite horizon case, with disks sufficiently large so that no infinite length free flight is possible. In this case the diffusion is normal, with $\hat{x}(t)^2$ growing like t. We shall return to the anomalous diffusion case in sect. 23.3.

ask J.-P. Eckmann for permission to use his figures

As we will work with three kinds of phase spaces, good manners require that we repeat what hats, tildas and nothings atop symbols signify:

$$\begin{array}{ll} \tilde{} & \text{fundamental domain, triangle in figure 23.2} \\ & \text{elementary cell, hexagon in figure 23.2} \\ \hat{} & \text{full phase space, lattice in figure 23.2} \end{array} \tag{23.1}$$

It is convenient to define an evolution operator for each of the 3 cases of figure 23.2. $\hat{x}(t) = \hat{f}^t(\hat{x})$ denotes the point in the global space $\hat{\mathcal{M}}$ reached by the flow in time t. $x(t) = f^t(x_0)$ denotes the corresponding flow in the elementary cell; the two are related by

$$\hat{n}_t(x_0) = \hat{f}^t(x_0) - f^t(x_0) \in T\,, \tag{23.2}$$

the translation of the endpoint of the global path into the elementary cell $\mathcal{M}$. The quantity $\tilde{x}(t) = \tilde{f}^t(\tilde{x})$ denotes the flow in the fundamental domain $\widetilde{\mathcal{M}}$; $\tilde{f}^t(\tilde{x})$ is related to $f^t(\tilde{x})$ by a discrete symmetry $g \in G$ which maps $\tilde{x}(t) \in \widetilde{\mathcal{M}}$ to $x(t) \in \mathcal{M}$.

☞ chapter 22

Fix a vector $\beta \in \mathbb{R}^d$, where d is the dimension of the phase space. We will compute the diffusive properties of the Lorentz gas from the leading eigenvalue of the evolution operator (10.11)

$$s(\beta) = \lim_{t\to\infty} \frac{1}{t} \log \langle e^{\beta\cdot(\hat{x}(t)-x)} \rangle_{\mathcal{M}}\ , \tag{23.3}$$

where the average is over all initial points in the elementary cell, $x \in \mathcal{M}$.

If all odd derivatives vanish by symmetry, there is no drift and the second derivatives

$$\left.\frac{\partial}{\partial \beta_i}\frac{\partial}{\partial \beta_j} s(\beta)\right|_{\beta=0} = \lim_{t\to\infty} \frac{1}{t}\langle(\hat{x}(t)-x)_i(\hat{x}(t)-x)_j\rangle_{\mathcal{M}} \ ,$$

yield a (generally anisotropic) diffusion matrix. The spatial diffusion constant is then given by the Einstein relation (10.13)

$$D = \frac{1}{2d}\sum_i \left.\frac{\partial^2}{\partial \beta_i^2} s(\beta)\right|_{\beta=0} = \lim_{t\to\infty} \frac{1}{2dt}\langle(\hat{q}(t)-q)^2\rangle_{\mathcal{M}} \quad ,$$

where the i sum is restricted to the spatial components q_i of the phase space vectors $x = (q,p)$, that is, if the dynamics is Hamiltonian to the number of the degrees of freedom.

reinstate mass, velocity, size to get β, m, σ dependencies right

We now turn to the connection between (23.3) and periodic orbits in the elementary cell. As the full $\hat{\mathcal{M}} \to \widetilde{\mathcal{M}}$ reduction is complicated by the nonabelian nature of G, we shall introduce the main ideas in the abelian $\hat{\mathcal{M}} \to \mathcal{M}$ context.

☞ remark 23.6

23.1.1 Reduction from $\hat{\mathcal{M}}$ to $\mathcal{M}$

The key idea follows from inspection of the relation

$$\left\langle e^{\beta\cdot(\hat{x}(t)-x)}\right\rangle_{\mathcal{M}} = \frac{1}{|\mathcal{M}|}\int_{\substack{x\in\mathcal{M}\\ \hat{y}\in\hat{\mathcal{M}}}} dx d\hat{y}\, e^{\beta\cdot(\hat{y}-x)}\delta(\hat{y}-\hat{f}^t(x)) \ .$$

$|\mathcal{M}| = \int_{\mathcal{M}} dx$ is the volume of the elementary cell $\mathcal{M}$. As in sect. 10.2, we have used the identity $1 = \int_{\mathcal{M}} dy\, \delta(y-\hat{x}(t))$ to motivate the introduction of the evolution operator $\mathcal{L}^t(\hat{y}, x)$. There is a unique lattice translation $\hat{n}$ such that $\hat{y} = y - \hat{n}$, with $y \in \mathcal{M}$, and $f^t(x)$ given by (23.2). The difference is a translation by a constant, and the Jacobian for changing integration from $d\hat{y}$ to dy equals unity. Therefore, and this is the main point, translation invariance can be used to reduce this average to the elementary cell:

$$\langle e^{\beta\cdot(\hat{x}(t)-x)}\rangle_{\mathcal{M}} = \frac{1}{|\mathcal{M}|}\int_{x,y\in\mathcal{M}} dx dy\, e^{\beta\cdot(\hat{f}^t(x)-x)}\delta(y-f^t(x)) \ . \quad (23.4)$$

As this is a translation, the Jacobian is $\delta\hat{y}/\delta y = 1$. In this way the global $\hat{f}^t(x)$ flow averages can be computed by following the flow $f^t(x_0)$ restricted to the elementary cell $\mathcal{M}$. The equation (23.4) suggests that we study the evolution operator

$$\mathcal{L}^t(y,x) = e^{\beta\cdot(\hat{x}(t)-x)}\delta(y-f^t(x)) \ , \quad (23.5)$$

where $\hat{x}(t) = \hat{f}^t(x) \in \hat{\mathcal{M}}$, but $x,\ f^t(x),\ y \in \mathcal{M}$. It is straightforward to check that this operator satisfies the semigroup property (10.25), $\int_{\mathcal{M}} dz\, \mathcal{L}^{t_2}(y,z)\mathcal{L}^{t_1}(z,x) = \mathcal{L}^{t_2+t_1}(y,x)$. For $\beta = 0$, the operator (23.5) is the Perron-Frobenius operator (9.10), with the leading eigenvalue $e^{s_0} = 1$ because there is no escape from this system (this will lead to the flow conservation sum rule (19.11) later on).

standing orbit!Lorentz gas
running orbits!Lorentz gas
accelerator mode

The rest is old hat. The spectrum of $\mathcal{L}$ is evaluated by taking the trace

☞ sect. 14.3

$$\mathrm{tr}\,\mathcal{L}^t = \int_{\mathcal{M}} dx\, e^{\beta\cdot\hat{n}_t(x)}\delta(x - x(t)) \,.$$

Here $\hat{n}_t(x)$ is the discrete lattice translation defined in (23.2). Two kinds of orbits periodic in the elementary cell contribute. A periodic orbit is called *standing* if it is also periodic orbit of the infinite phase space dynamics, $\hat{f}^{T_p}(x) = x$, and it is called *running* if it corresponds to a lattice translation in the dynamics on the infinite phase space, $\hat{f}^{T_p}(x) = x + \hat{n}_p$. In the theory of area–preserving maps such orbits are called *accelerator modes*, as the diffusion takes place along the momentum rather than the position coordinate. The travelled distance $\hat{n}_p = \hat{n}_{T_p}(x_0)$ is independent of the starting point x_0, as can be easily seen by continuing the path periodically in $\hat{\mathcal{M}}$.

recheck usage “standing”, “running” with the literature.

explain that “accelerator modes” makes sense for standard map

The final result is the spectral determinant (15.7)

$$\det\left(s(\beta) - \mathcal{A}\right) = \prod_p \exp\left(-\sum_{r=1}^{\infty} \frac{1}{r} \frac{e^{(\beta\cdot\hat{n}_p - sT_p)r}}{\left|\det\left(\mathbf{1} - \mathbf{J}_p^r\right)\right|}\right) , \qquad (23.6)$$

or the corresponding dynamical zeta function (15.16)

$$1/\zeta(\beta, s) = \prod_p \left(1 - \frac{e^{(\beta\cdot\hat{n}_p - sT_p)}}{|\Lambda_p|}\right) . \qquad (23.7)$$

The dynamical zeta function cycle averaging formula (18.17) for the diffusion constant (10.13), zero mean drift $\langle\hat{x}_i\rangle = 0$, is given by

$$D = \frac{1}{2d}\frac{\langle\hat{x}^2\rangle_\zeta}{\langle T\rangle_\zeta} = \frac{1}{2d}\frac{1}{\langle T\rangle_\zeta}{\sum}' \frac{(-1)^{k+1}(\hat{n}_{p_1} + \cdots + \hat{n}_{p_k})^2}{|\Lambda_{p_1}\cdots\Lambda_{p_k}|} . \qquad (23.8)$$

where the sum is over all distinct non-repeating combination of prime cycles. The derivation is standard, still the formula is strange. Diffusion is unbounded motion accross an infinite lattice; nevertheless, the reduction to the elementary cell enables us to compute relevant quantities in the usual way, in terms of periodic orbits.

A sleepy reader might protest that $x_p = x(T_p) - x(0)$ is manifestly equal to zero for a periodic orbit. That is correct; $\hat{n}_p$ in the above formula refers to a displacement on the *infinite* periodic lattice, while p refers to closed orbit of the dynamics reduced to the elementary cell, with x_p belonging to the closed prime cycle p.

Even so, this is not an obvious formula. Globally periodic orbits have $\hat{x}_p^2 = 0$, and contribute only to the time normalization $\langle T \rangle_\zeta$. The mean square displacement $\left\langle \hat{x}^2 \right\rangle_\zeta$ gets contributions only from the periodic runaway trajectories; they are closed in the elementary cell, but on the periodic lattice each one grows like $\hat{x}(t)^2 = (\hat{n}_p/T_p)^2 = v_p^2 t^2$. So the orbits that contribute to the trace formulas and spectral determinants exhibit either ballistic transport or no transport at all: diffusion arises as a balance between the two kinds of motion, weighted by the $1/|\Lambda_p|$ measure. If the system is not hyperbolic such weights may be abnormally large, with $1/|\Lambda_p| \approx 1/{T_p}^\alpha$ rather than $1/|\Lambda_p| \approx e^{-T_p \lambda}$, where λ is the Lyapunov exponent, and they may lead to anomalous diffusion - accelerated or slowed down depending on whether the probabilities of the running or the standing orbits are enhanced.

☞ sect. 23.3

We illustrate the main idea, tracking of a globally diffusing orbit by the associated confined orbit restricted to the elementary cell, with a class of simple 1-d dynamical systems where all transport coefficients can be evaluated analytically. We return to the Lorentz gas in sect. 23.4.

⇓PRELIMINARY
⇑PRELIMINARY

23.2 Diffusion induced by chains of 1-d maps

In a typical deterministic diffusive process, trajectories originating from a given scatterer reach a finite set of neighboring scatterers in one bounce, and then the process is repeated. As was shown in chapter 11, the essential part of this process is the stretching along the unstable directions of the flow, and in the crudest approximation the dynamics can be modelled by 1-d expanding maps. This observation motivates introduction of a class of particularly simple 1-d systems, chains of piecewise linear maps.

We start by defining the map $\hat{f}$ on the unit interval as

$$\hat{f}(\hat{x}) = \begin{cases} \Lambda\hat{x} & \hat{x} \in [0, 1/2) \\ \Lambda\hat{x} + 1 - \Lambda & \hat{x} \in (1/2, 1] \end{cases} , \qquad \Lambda > 2 , \tag{23.9}$$

and then extending the dynamics to the entire real line, by imposing the translation property

$$\hat{f}(\hat{x} + \hat{n}) = \hat{f}(\hat{x}) + \hat{n} \qquad \hat{n} \in \mathbb{Z} . \tag{23.10}$$

As the map is dicontinuous at $\hat{x} = 1/2$, $\hat{f}(1/2)$ is undefined, and the $x = 1/2$ point has to be excluded from the Markov partition. The map is antisymmetric under the $\hat{x}$-coordinate flip

$$\hat{f}(\hat{x}) = -\hat{f}(-\hat{x}) , \tag{23.11}$$

critical!value

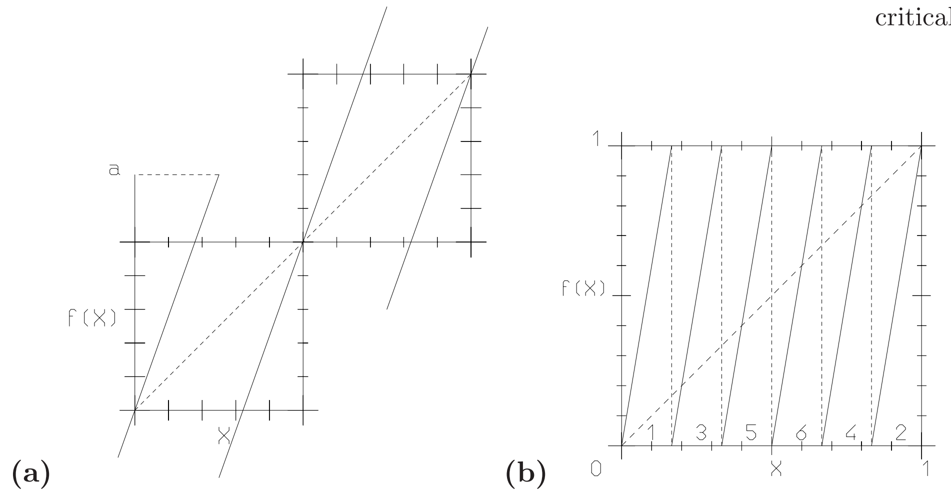

Figure 23.3: (a) $\hat{f}(\hat{x})$, the full space sawtooth map (23.9), $\Lambda > 2$. (b) $f(x)$, the sawtooth map restricted to the unit circle (23.12), $\Lambda = 6$.

so the dynamics will exhibit no mean drift; all odd derivatives of the generating function (10.11) with respect to β, evaluated at $\beta = 0$, will vanish.

The map (23.9) is sketched in figure 23.3(a). Initial points sufficiently close to either of the fixed points in the initial unit interval remain in the elementary cell for one iteration; depending on the slope Λ, other points jump $\hat{n}$ cells, either to the right or to the left. Repetition of this process generates a random walk for almost every initial condition.

The translational symmetry (23.10) relates the unbounded dynamics on the real line to dynamics restricted to the elementary cell - in the example at hand, the unit interval curled up into a circle. Associated to $\hat{f}(\hat{x})$ we thus also consider the circle map

$$f(x) = \hat{f}(\hat{x}) - \left[\hat{f}(\hat{x})\right] , \qquad x = \hat{x} - [\hat{x}] \in [0,1] \tag{23.12}$$

define $\hat{n}$ here as well

figure 23.3(b), where $[\cdots]$ stands for the integer part (23.2). As noted above, the elementary cell cycles correspond to either standing or running orbits for the map on the full line: we shall refer to $\hat{n}_p \in \mathbb{Z}$ as the *jumping number* of the p cycle, and take as the cycle weight

$$t_p \,=\, z^{n_p} e^{\beta \hat{n}_p} / |\Lambda_p| \,. \tag{23.13}$$

For the piecewise linear map of figure 23.3 we can evaluate the dynamical zeta function in closed form. Each branch has the same value of the slope, and the map can be parametrized by a single parameter, for example its critical value $a = \hat{f}(1/2)$, the absolute maximum on the interval $[0,1]$ related to the slope of the map by $a = \Lambda/2$. The larger Λ is, the stronger is the stretching action of the map.

The diffusion constant formula (23.8) for 1-d maps is

$$D = \frac{1}{2}\frac{\langle \hat{n}^2 \rangle_\zeta}{\langle n \rangle_\zeta} \tag{23.14}$$

where the "mean cycle time" is given by (18.18)

$$\langle n \rangle_\zeta = z\frac{\partial}{\partial z}\frac{1}{\zeta(0,z)}\bigg|_{z=1} = -\sum{}'(-1)^k \frac{n_{p_1} + \cdots + n_{p_k}}{|\Lambda_{p_1}\cdots\Lambda_{p_k}|}, \tag{23.15}$$

and the "mean cycle displacement squared" by (20.1)

$$\langle \hat{n}^2 \rangle_\zeta = \frac{\partial^2}{\partial \beta^2}\frac{1}{\zeta(\beta,1)}\bigg|_{\beta=0} = -\sum{}'(-1)^k \frac{(\hat{n}_{p_1} + \cdots + \hat{n}_{p_k})^2}{|\Lambda_{p_1}\cdots\Lambda_{p_k}|}, \tag{23.16}$$

the primed sum indicating all distinct non-repeating combinations of prime cycles. The evaluation of these formulas in this simple system will require nothing more than pencil and paper.

23.2.1 Case of unrestricted symbolic dynamics

Whenever Λ is an integer number, the symbolic dynamics is exceedingly simple. For example, for the case $\Lambda = 6$ illustrated in figure 23.3(b), the elementary cell map consists of 6 full branches, with uniform stretching factor $\Lambda = 6$. The branches have different jumping numbers: for branches 1 and 2 we have $\hat{n} = 0$, for branch 3 we have $\hat{n} = +1$, for branch 4 $\hat{n} = -1$, and finally for branches 5 and 6 we have respectively $\hat{n} = +2$ and $\hat{n} = -2$. The same structure reappears whenever Λ is an even integer $\Lambda = 2a$: all branches are mapped onto the whole unit interval and we have two $\hat{n} = 0$ branches, one branch for which $\hat{n} = +1$ and one for which $\hat{n} = -1$, and so on, up to the maximal jump $|\hat{n}| = a - 1$. The symbolic dynamics is thus full, unrestricted shift in $2a$ symbols $\{0_+, 1_+, \ldots, (a-1)_+, (a-1)_-, \ldots, 1_-, 0_-\}$, where the symbol indicates both the length and the direction of the corresponding jump.

For the piecewise linear maps with uniform stretching the weight associated with a given symbol sequence is a product of weights for individual steps, $t_{sq} = t_s t_q$. For the map of figure 23.3 there are 6 distinct weigths (23.13):

$$\begin{aligned} t_1 &= t_2 = z/\Lambda \\ t_3 &= e^{\beta} z/\Lambda\,, \quad t_4 = e^{-\beta} z/\Lambda\,, \quad t_5 = e^{2\beta} z/\Lambda\,, \quad t_6 = e^{-2\beta} z/\Lambda\,. \end{aligned}$$

The piecewise linearity and the simple symbolic dynamics lead to the full cancellation of all curvature corrections in (18.5). The *exact* dynamical zeta function (13.13) is given by the fixed point contributions:

why not 1/2 cosh?

$$\begin{aligned} 1/\zeta(\beta,z) &= 1 - t_{0_+} - t_{0_-} - \cdots - t_{(a-1)_+} - t_{(a-1)_-} \\ &= 1 - \frac{z}{a}\left(1 + \sum_{j=1}^{a-1}\cosh(\beta j)\right). \end{aligned} \tag{23.17}$$

kurtosis
Helfand moments
Gaussian!integral

The leading (and only) eigenvalue of the evolution operator (23.5) is

$$s(\beta) = \log\left\{\frac{1}{a}\left(1 + \sum_{j=1}^{a-1}\cosh(\beta j)\right)\right\}, \qquad \Lambda = 2a,\ a \text{ integer}. \tag{23.18}$$

The flow conservation (19.11) sum rule is manifestly satisfied, so $s(0) = 0$. The first derivative $s(0)'$ vanishes as well by the left/right symmetry of the dynamics, implying vanishing mean drift $\langle \hat{x} \rangle = 0$. The second derivative $s(\beta)''$ yields the diffusion constant (23.14):

$$\langle n \rangle_\zeta = 2a\frac{1}{\Lambda} = 1, \qquad \left\langle \hat{x}^2 \right\rangle_\zeta = 2\frac{0^2}{\Lambda} + 2\frac{1^2}{\Lambda} + 2\frac{2^2}{\Lambda} + \cdots + 2\frac{(a-1)^2}{\Lambda} \tag{23.19}$$

Using the identity $\sum_{k=1}^n k^2 = n(n+1)(2n+1)/6$ we obtain

$$D = \frac{1}{24}(\Lambda-1)(\Lambda-2), \qquad \Lambda \text{ even integer}. \tag{23.20}$$

Similar calculation for odd integer $\Lambda = 2k-1$ yields

23.1
page 458

$$D = \frac{1}{24}(\Lambda^2-1), \qquad \Lambda \text{ odd integer}. \tag{23.21}$$

23.2.2 Higher order transport coefficients

The same approach yields higher order transport coefficients

harmonize with the averages chapter

$$\mathcal{B}_k = \frac{1}{k!}\frac{d^k}{d\beta^k}s(\beta)\Big|_{\beta=0}, \qquad \mathcal{B}_2 = D, \tag{23.22}$$

known for $k > 2$ as the Burnett coefficients. The behavior of the higher order coefficients yields information on the relaxation to the asymptotic distribution function generated by the diffusive process. Here $\hat{x}_t$ is the relevant dynamical variable and $\mathcal{B}_k$'s are related to moments $\left\langle \hat{x}_t^k \right\rangle$ of arbitrary order.

discuss Kulso (??) formula

Were the diffusive process purely Gaussian

recheck

$$e^{ts(\beta)} = \frac{1}{\sqrt{4\pi Dt}}\int_{-\infty}^{+\infty} d\hat{x}\, e^{\beta\hat{x}} e^{-\hat{x}^2/(4Dt)} = e^{\beta^2 Dt} \tag{23.23}$$

Burnett coefficient
Markov!partition

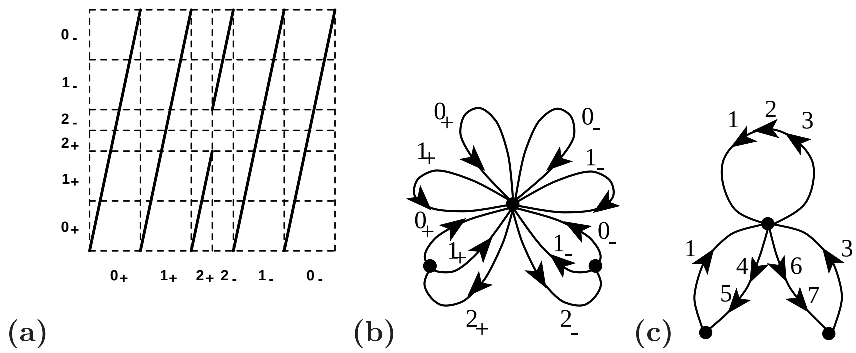

Figure 23.4: (a) A partition of the unit interval into six intervals, labeled by the jumping number $\hat{n}(x)$ $I = \{0_+, 1_+, 2_+, 2_-, 1_-, 0_-\}$. The partition is Markov, as the critical point is mapped onto the right border of $\mathcal{M}_{1_+}$. (b) The Markov graph for this partition. (c) The Markov graph in the compact notation of (23.26) (introduced by Vadim Moroz).

the only $\mathcal{B}_k$ coefficient different from zero would be $\mathcal{B}_2 = D$. Hence, nonvanishing higher order coefficients signal deviations of deterministic diffusion from a Gaussian stochastic process.

For the map under consideration the first Burnett coefficient coefficient $\mathcal{B}_4$ is easily evaluated. For example, using (23.18) in the case of even integer slope $\Lambda = 2a$ we obtain

23.2
page 458

$$\mathcal{B}_4 = -\frac{1}{4! \cdot 60}(a-1)(2a-1)(4a^2 - 9a + 7)\,. \tag{23.24}$$

We see that deterministic diffusion is <u>not</u> a Gaussian stochastic process. Higher order even coefficients may be calculated along the same lines.

23.2.3 Case of finite Markov partitions

For piecewise-linear maps exact results may be obtained whenever the critical points are mapped in finite numbers of iterations onto partition boundary points, or onto unstable periodic orbits. We will work out here an example for which this occurs in two iterations, leaving other cases as exercises.

fix figure 23.4(c)
credits in acknowledgements

The key idea is to construct a *Markov partition* (11.4), with intervals mapped *onto* unions of intervals. As an example we determine a value of the parameter $4 \le \Lambda \le 6$ for which $f(f(1/2)) = 0$. As in the integer Λ case, we partition the unit interval into six intervals, labeled by the jumping number $\hat{n}(x) \in \{\mathcal{M}_{0_+}, \mathcal{M}_{1_+}, \mathcal{M}_{2_+}, \mathcal{M}_{2_-}, \mathcal{M}_{1_-}, \mathcal{M}_{0_-}\}$, ordered by their placement along the unit interval, figure 23.4(a).

In general the critical value $a = \hat{f}(1/2)$ will not correspond to an interval border, but now we choose a such that the critical point is mapped onto the right border of $\mathcal{M}_{1_+}$. Equating $f(1/2)$ with the right border of $\mathcal{M}_{1_+}$, $x = 1/\Lambda$, we obtain a quadratic equation with the expanding solution $\Lambda = 2(\sqrt{2}+1)$. For this parameter value $f(\mathcal{M}_{1_+}) = \mathcal{M}_{0_+} \bigcup \mathcal{M}_{1_+}$, $f(\mathcal{M}_{2_-}) = \mathcal{M}_{0_-} \bigcup \mathcal{M}_{1_-}$, while the remaining intervals map onto the whole unit interval $\mathcal{M}$. The transition matrix (11.2) is given by

$$\phi' = T\phi \; = \; \begin{pmatrix} 1 & 1 & 1 & 0 & 1 & 1 \\ 1 & 1 & 1 & 0 & 1 & 1 \\ 1 & 1 & 0 & 0 & 1 & 1 \\ 1 & 1 & 0 & 0 & 1 & 1 \\ 1 & 1 & 0 & 1 & 1 & 1 \\ 1 & 1 & 0 & 1 & 1 & 1 \end{pmatrix} \begin{pmatrix} \phi_{0_+} \\ \phi_{1_+} \\ \phi_{2_+} \\ \phi_{2_-} \\ \phi_{1_-} \\ \phi_{0_-} \end{pmatrix} . \tag{23.25}$$

One could diagonalize (23.25) on a computer, but, as we saw in sect. 11.5, the Markov graph figure 23.4(b) corresponding to figure 23.4(a) offers more insight into the dynamics. The graph figure 23.4(b) can be redrawn more compactly as Markov graph figure 23.4(c) by replacing parallel lines in a graph by their sum

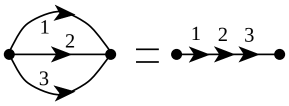

$$= t_1 + t_2 + t_3 \,. \tag{23.26}$$

The dynamics is unrestricted in the alphabet

$$\mathcal{A} = \{0_+,\, 1_+,\, 2_+0_+,\, 2_+1_+,\, 2_-1_-,\, 2_-0_-,\, 1_-,\, 0_-\}\,.$$

Applying the loop expansion (13.13) of sect. 13.3, we are led to the dynamical zeta function

$$\begin{aligned} 1/\zeta(\beta,z) &= 1 - t_{0_+} - t_{1_+} - t_{2_+0_+} - t_{2_+1_+} - t_{2_-1_-} - t_{2_-0_-} - t_{1_-} - t_{0_-} \\ &= 1 - \frac{2z}{\Lambda}\,(1+\cosh(\beta)) - \frac{2z^2}{\Lambda^2}\,(\cosh(2\beta)+\cosh(3\beta)) \end{aligned} \tag{23.27}$$

For grammar as simple as this one, the dynamical zeta function is the sum over fixed points of the unrestricted alphabet. As the first check of this expression for the dynamical zeta function we verify that

$$1/\zeta(0,1) \, = 1 - \frac{4}{\Lambda} - \frac{4}{\Lambda^2} \, = \, 0\,,$$

as required by the flow conservation (19.11). Conversely, we could have started by picking the desired Markov partition, writing down the corresponding dynamical zeta function, and then fixing Λ by the $1/\zeta(0,1) = 0$ condition. For more complicated Markov graphs this approach, together with the factorization (23.36), is helpful in reducing the order of the polynomial condition that fixes Λ.

structural stability
stability!structural

The diffusion constant follows from (23.14)

23.3
page 458

$$\begin{aligned} \langle n \rangle_\zeta &= 4\frac{1}{\Lambda} + 4\frac{2}{\Lambda^2}\,, \quad \langle \hat{n}^2 \rangle_\zeta = 2\frac{1^2}{\Lambda} + 2\frac{2^2}{\Lambda^2} + 2\frac{3^2}{\Lambda^2} \\ D &= \frac{15+2\sqrt{2}}{16+8\sqrt{2}}\,. \end{aligned} \tag{23.28}$$

It is by now clear how to build an infinite hierarchy of finite Markov partitions: tune the slope in such a way that the critical value $f(1/2)$ is mapped into the fixed point at the origin in a finite number of iterations p $f^P(1/2) = 0$. By taking higher and higher values of p one constructs a dense set of Markov parameter values, organized into a hierarchy that resembles the way in which rationals are densely embedded in the unit interval. For example, each of the 6 primary intervals can be subdivided into 6 intervals obtained by the 2-nd iterate of the map, and for the critical point mapping into any of those in 2 steps the grammar (and the corresponding cycle expansion) is finite. So, if we can prove continuity of $D = D(\Lambda)$, we can apply the periodic orbit theory to the sawtooth map (23.9) for a random "generic" value of the parameter Λ, for example $\Lambda = 4.5$. The idea is to bracket this value of Λ by a sequence of nearby Markov values, compute the exact diffusion constant for each such Markov partition, and study their convergence toward the value of D for $\Lambda = 4.5$. ⇓PRELIMINARY Some details of how this is accomplished are given in appendix F.2 for a related problem, the pruned Bernulli shift. ⇑PRELIMINARY Judging how difficult such problem is already for a tent map (see sect. 13.6 and appendix F.1), this is not likely to take only a week of work.

Expressions like (23.20) may lead to an expectation that the diffusion coefficient (and thus transport properties) are smooth functions of parameters controling the chaoticity of the system. For example, one might expect that the diffusion coefficient increases smoothly and monotonically as the slope Λ of the map (23.9) is increased, or, perhaps more physically, that the diffusion coefficient is a smooth function of the Lyapunov exponent λ. This turns out not to be true: D as a function of Λ is a fractal, nowhere differentiable curve illustrated in figure 23.5. The dependence of D on the map parameter Λ is rather unexpected - even though for larger Λ more points are mapped outside the unit cell in one iteration, the diffusion constant does not necessarily grow.

This is a consequence of the lack of structural stability, even of purely hyperbolic systems such as the Lozi map and the 1-d diffusion map (23.9). The trouble arises due to non-smooth dependence of the topological entropy on system parameters - any parameter change, no mater how small, leads to creation and destruction of ininitely many periodic orbits. As far as diffusion is concerned this means that even though local expansion rate is a smooth function of Λ, the number of ways in which the trajectory can re-enter the the initial cell is an irregular function of Λ.

The lesson is that lack of structural stabily implies lack of spectral stability, and no global observable is expected to depend smoothly on the

spectral stability
stability!spectral
anomalous diffusion
diffusion!anomalous

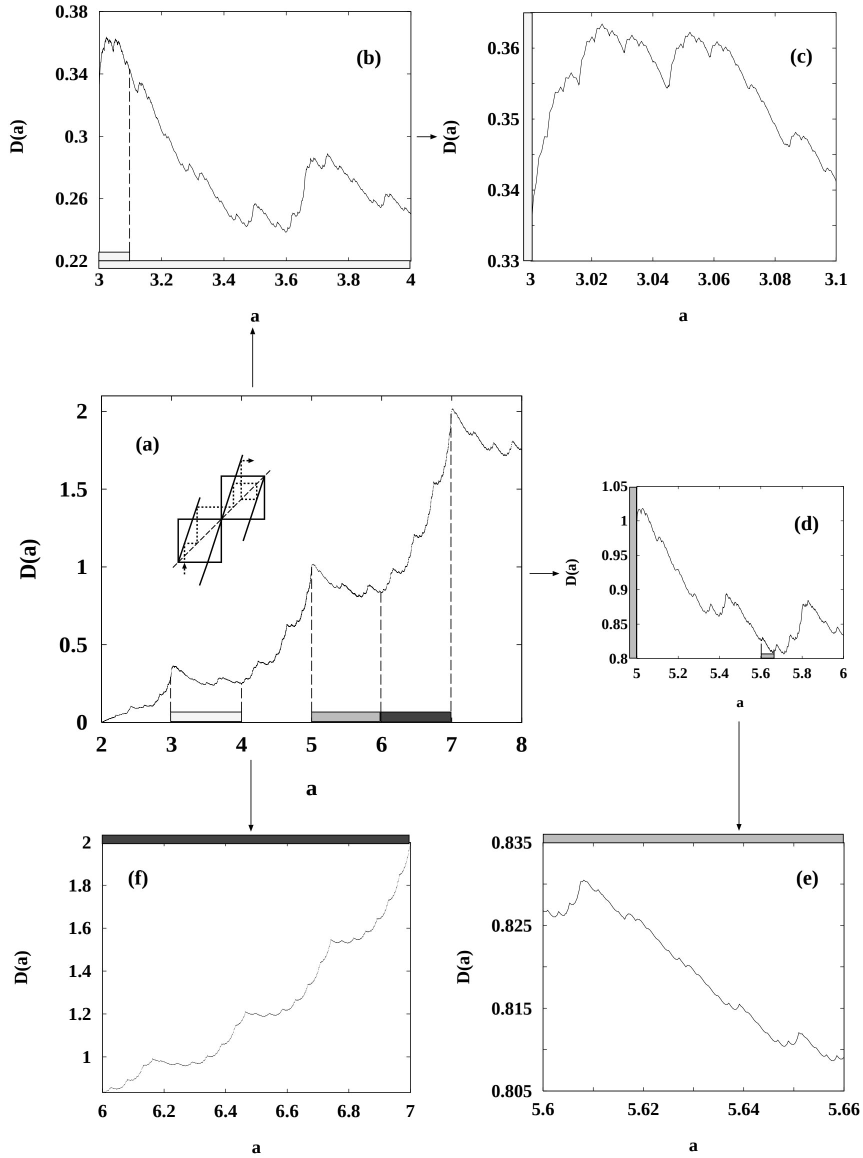

Figure 23.5: The dependence of D on the map parameter a is continuous, but not monotone. (From ref. [23.7]). Here a stands for the slope Λ in (23.9).

system parameters. If you want to master the material, working through the project S.1 and/or project S.2 is strongly recommended.

23.3 Marginal stability and anomalous diffusion

What effect does the intermittency of chapter 21 have on transport properties of 1-d maps? Consider a $1-d$ map of the real line on itself with the same properties as in sect. 23.2, except for a marginal fixed point at $x = 0$.

A marginal fixed point unbalances the role of running and standing orbits, thus generating a mechanism that may result in anomalous diffusion. Our model example is the map shown in figure 23.6(a), with the corresponding circle map shown in figure 23.6(b). As in sect. 21.2.1, a branch

Jonqui‘‘‘ere function

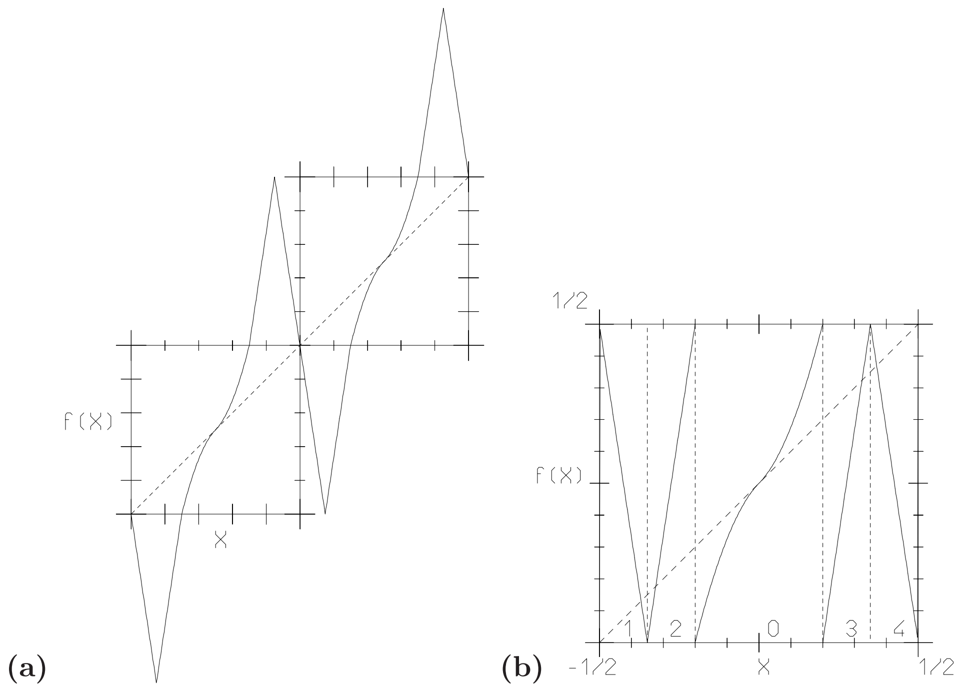

Figure 23.6: (a) A map with marginal fixed point. (b) The map restricted to the unit circle.

with support in $\mathcal{M}_i$, $i = 1,2,3,4$ has constant slope Λ_i, while $f|_{\mathcal{M}_0}$ is of intermittent form. To keep you nimble, this time we take a slightly different choice of slopes. The toy example of sect. 21.2.1 was cooked up so that the $1/s$ branch cut in dynamical zeta function was the whole answer. Here we shall take a slightly different route, and pick piecewise constant slopes such that the dynamical zeta function for intermittent system can be expressed in terms of the Jonquière function

remark 23.8

$$J(z,s) = \sum_{k=1}^{\infty} z^k/k^s \tag{23.29}$$

Once the $\overline{0}$ fixed point is pruned away, the symbolic dynamics is given by the infinite alphabet $\{1,2,3,4,0^i1,0^j2,0^k3,0^l4\}$, $i,j,k,l = 1,2,\ldots$ (compare with table 21.1). The partitioning of the subinterval $\mathcal{M}_0$ is induced by $\mathcal{M}_{0^k(right)} = \phi^k_{(right)}(\mathcal{M}_3 \bigcup \mathcal{M}_4)$ (where $\phi_{(right)}$ denotes the inverse of the right branch of $\hat{f}|_{\mathcal{M}_0}$) and the same reasoning applies to the leftmost branch. These are regions over which the slope of $\hat{f}|_{\mathcal{M}_0}$ is constant. Thus we have the following stabilities and jumping numbers associated to letters:

$$\begin{array}{rll} 0^k3,\ 0^k4 & \Lambda_p = \frac{k^{1+\alpha}}{q/2} & \hat{n}_p = 1 \\ 0^l1,\ 0^l2 & \Lambda_p = \frac{l^{1+\alpha}}{q/2} & \hat{n}_p = -1 \\ 3,\ 4 & \Lambda_p = \pm\Lambda & \hat{n}_p = 1 \\ 2,\ 1 & \Lambda_p = \pm\Lambda & \hat{n}_p = -1\,, \end{array} \tag{23.30}$$

where $\alpha = 1/s$ is determined by the intermittency exponent (21.1), while q

is to be determined by the flow conservation (19.11) for $\hat{f}$: —PCdefine R dropped R from Roberto's ζ_R

$$\frac{4}{\Lambda} + 2q\zeta(\alpha+1) = 1$$

so that $q = (\Lambda - 4)/2\Lambda\zeta(\alpha+1)$. The dynamical zeta function picks up contributions just by the alphabet's letters, as we have imposed piecewise linearity, and can be expressed in terms of a Jonguiere function (23.29): dropped R from ζ_R

$$1/\zeta_0(z,\beta) \;=\; 1 - \frac{4}{\Lambda} z\cosh\beta - \frac{\Lambda-4}{\Lambda\zeta(1+\alpha)} z\cosh\beta \cdot J(z,\alpha+1)\,. \tag{23.31}$$

Its first zero $z(\beta)$ is determined by

$$\frac{4}{\Lambda} z + \frac{\Lambda-4}{\Lambda\zeta(1+\alpha)} z \cdot J(z,\alpha+1) \;=\; \frac{1}{\cosh\beta}\,.$$

By using implicit function derivation we see that D vanishes (that is, $z''(\beta)|_{\beta=1} = 0$) when $\alpha \leq 1$. The physical interpretion is that a typical orbit will stick for long times near the $\overline{0}$ marginal fixed point, and the 'trapping time' will be larger for higher values of the intermittency parameter s (recall $\alpha = s^{-1}$). Hence, we need to look more closely at the behavior of traces of high powers of the transfer operator.

The evaluation of transport coefficient requires one more derivative with respect to expectation values of phase functions (see sect. 23.1): if we use the diffusion dynamical zeta function (23.7), we may write the diffusion coefficient as an inverse Laplace transform,in such a way that any distinction between maps and flows has vanished. In the case of 1-d diffusion we thus have

phase?

⇓PRELIMINARY

21.4

page 409

⇑PRELIMINARY

$$D \;=\; \lim_{t\to\infty} \frac{d^2}{d\beta^2} \frac{1}{2\pi i} \int_{a-i\infty}^{a+i\infty} ds\, e^{st} \frac{\zeta'(\beta,s)}{\zeta(\beta,s)}\bigg|_{\beta=0} \tag{23.32}$$

where the ζ' refers to the derivative with respect to s.

The evaluation of inverse Laplace transforms for high values of the argument is most conveniently performed using Tauberian theorems. We shall take

$$\omega(\lambda) \;=\; \int_0^\infty dx\, e^{-\lambda x} u(x)\,,$$

with $u(x)$ monotone as $x \to \infty$; then, as $\lambda \mapsto 0$ and $x \mapsto \infty$ respectively (and $\rho \in (0,\infty)$),

$$\omega(\lambda) \;\sim\; \frac{1}{\lambda^\rho} L\left(\frac{1}{\lambda}\right)$$

if and only if

$$u(x) \sim \frac{1}{\Gamma(\rho)} x^{\rho-1} L(x)\,,$$

where L denotes any slowly varying function with $\lim_{t\to\infty} L(ty)/L(t) = 1$. Now

$$\frac{1/{\zeta_0}'(e^{-s},\beta)}{1/\zeta_0(e^{-s},\beta)} = \frac{\left(\frac{4}{\Lambda} + \frac{\Lambda-4}{\Lambda\zeta(1+\alpha)}\left(J(e^{-s},\alpha+1) + J(e^{-s},\alpha)\right)\right)\cosh\beta}{1 - \frac{4}{\Lambda}e^{-s}\cosh\beta - \frac{\Lambda-4}{\Lambda\zeta(1+\alpha)} e^{-s}(e^{-s},\alpha+1)\cosh\beta J}\,.$$

why 0?

We then take the double derivative with respect to β and obtain

$$\frac{d^2}{d\beta^2}\left(1/{\zeta_0}'(e^{-s},\beta)/\zeta^{-1}(e^{-s},\beta)\right)_{\beta=0}$$

$$= \frac{\frac{4}{\Lambda} + \frac{\Lambda-4}{\Lambda\zeta(1+\alpha)}\left(J(e^{-s},\alpha+1) + J(e^{-s},\alpha)\right)}{\left(1 - \frac{4}{\Lambda}e^{-s} - \frac{\Lambda-4}{\Lambda\zeta(1+\alpha)} e^{-s} J(e^{-s},\alpha+1)\right)^2} = g_\alpha(s) \qquad (23.33)$$

The asymptotic behavior of the inverse Laplace transform (23.32) may then be evaluated via Tauberian theorems, once we use our estimate for the behavior of Jonquière functions near $z = 1$. The deviations from normal behavior correspond to an explicit dependence of D on time. Omitting prefactors (which can be calculated by the same procedure) we have

$$g_\alpha(s) \sim \begin{cases} s^{-2} & \text{for } \alpha > 1 \\ s^{-(\alpha+1)} & \text{for } \alpha \in (0,1) \\ 1/(s^2 \ln s) & \text{for } \alpha = 1\,. \end{cases}$$

23.6 page 458

The anomalous diffusion exponents follow:

$$\langle (x - x_0)^2 \rangle_t \sim \begin{cases} t & \text{for } \alpha > 1 \\ t^\alpha & \text{for } \alpha \in (0,1) \\ t/\ln t & \text{for } \alpha = 1\,. \end{cases} \qquad (23.34)$$

⇓PRELIMINARY

23.4 Lorentz gas

In economics, reflexivity runs counter to the notion of equilibrium which an free market system is supposed to tend towards. It is, indeed, the reason why open systems do not reach equilibrium but are prone to instability and self-increasing trends, cycles of boom and bust. Development is not linear but feeds on itself. Instead of balancing towards the point of equilibrium self-reinforcing trends create unstable far-from-equilibrium conditions.

George Soros, "The Crisis of Global Capitalism"

(L. Rondoni, R. Artuso and P. Cvitanović)

We now return to the problem of computing the diffusion coefficient for a "finite horizon" Lorentz gas on a hexagonal lattice introduced in sect. 23.1.

LR: Comment by Lamberto

We are not going to describe in full detail all the calculations that have performed for such a system, our main goal is to provide a physically relevant example where the symbolic dynamics is enormously complicated, and application of formulas like (23.8) is problematic. The complexity of symbolic dynamics for this system has a very clear and profound mathematical justification: Markov partitions for disperse billiards are made of an infinite countable collection of pieces, very unevenly sized. The source of troubles are the grazing singularities, corresponding to the orbits that are tangent to a disk: a cone of trajectories close to the tangent one is split into two pieces at the tangency point, and the process repeats at every tangency. This mechanism causes the global unstable and stable manifolds to consist of a countable number of smooth components. Thus the presence of singularities in a sense weakens the strong chaotic properties induced by complete hyperbolicity (due to the fact that any single collision leads to defocusing, and that the fime between two successive collisions if bounded from above by a finite quantity).

Let us first define the parameters of the model: we set the disk radius $R = 1$ and denote by w the disk to disk distance, so that the centers of two neighboring disks are separated by a distance $2+w$. For a hexagonal lattice we require $0 \leq w \leq 4/\sqrt{3} - 2$ in order that the finite horizon condition be satisfied.

23.4.1 Lorentz gas: symbolic dynamics

If we start a trajectory from any scatterer in the lattice, under the condition of finite horizon, there are two possibilities for the next hit: either it takes place on one of the six neighboring disks, or on one of the six next-to-nearest disks. Hence we may introduce an alphabet, by labeling these disks clockwise from 0 to 11: if we assign the label 0 to one of the closest obstacles, even labels will then correspond to short flights, see figure 23.7.

Then, any trajectory (without grazing collisions) may be uniquely identified by assigning one of these twelve symbols to each free flight. The way this is done is to let the symbol for a free flight depend on the vector separation between initial and final point of such a segment of trajectory. Then, one should imagine that the center of figure 23.7 is always translated to the scatterer where the free flight starts, and that the symbol for the flight is the one of the scatterer where it ends. So, in practice, for a spacing $w = 0.3$, which is just below the finite horizon condition, one has only four types of cycles with two collisions, that is, orbits which indefinitely repeat the same symbol sequence of two symbols: the are of course short orbits between two neighboring scatterers, like (0 6) (next neighbors) or (1 7) (next to nearest neighbors), as well as (1 5) and (0 5) orbits. All these orbits belong to

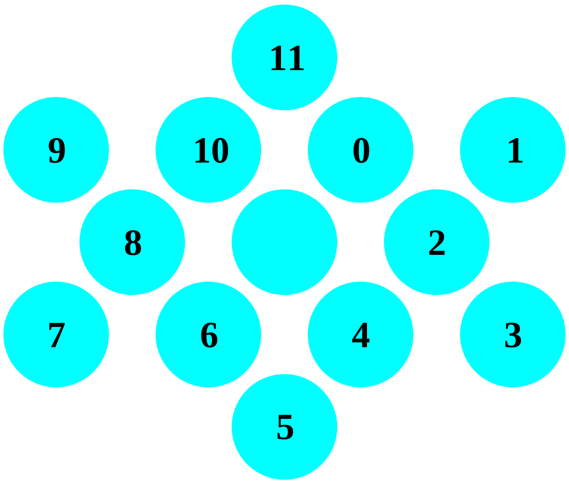

Figure 23.7: Symbolic dynamics for closely packed Lorentz gas.

Orbit	Degeneracy	$\tau\lambda$
(0 6)	3	1.51286399
(1 7)	3	3.51394510
(1 5)	6	4.65944481
(0 5)	12	3.15831208
(0 4 8)	4	3.27128792
(0 2 7)	12	6.23520184
(0 2 6)	24	6.31880379
(0 2 5)	24	8.30080318

Table 23.1: Dynamical properties of length-2 and 3 cycles, at $w = 0.3$.

groups, characterized by the same layout, and differing just in the orientation: this is of course due to the symmetry propreties of the system: as the symmetry group is discrete there is a maximum number of different orbits in each group (which is 24 in the case under consideration). Obviously, the fact that the different orbits of one kind are oriented in different directions does not affect their length τ and their Lyapunov exponent λ, which are exactly the same for all orbits within one group. The number of distinct orbits within one group, and the corresponding product $\tau\lambda$, which appears in the definition of the stability eigenvalues are listed in table 23.1, for cycles of length 2 and 3.

23.5
page 458

It is clear from these considerations that not all possible symbol strings actually give rise to cycles. This is because the symbolic dynamics for the Lorentz gas is marred by a large amount of pruning. For instance, there is an obvious pruning rule that the same symbol cannot be repeated twice, as this would correspond to a trajectory crossing a disk. Many more pruning rules are present: for instance, in the dense gas we consider here not only a letter cannot repeat, but the next symbol has to vary at least by two units after a short flight, and by three units after a long flight. The immense amount of pruning present in the problem may be appreciated by looking at the second column of table 23.2, in which the number of cycles is reported as a function of cycle length: order by order we get roughly an increase by 3, instead of the factor 11 which would come from an unrestricted grammar (keeping into account only the non–crossing condition, which effectively

length	# cycles	$\zeta(0,0)$	λ	D
1	0	-	-	-
2	24	-0.31697	1.330	0.375
3	64	-0.54152	1.435	0.338
4	156	-0.09718	1.902	0.282
5	492	0.02383	2.324	0.212
6	1484	0.02812	1.931	0.129
7	5244	0.02044	1.836	0.185
8	19008	-0.00036	1.754	0.256
ref. [23.1], numerical experiment				0.25(1)
ref. [23.2], numerical experiment				0.2492(3)

Table 23.2: Elementary cell, w=0.3. The cycles are sorted with the method of remark T.9. The last column is taken from ref. [23.2].

reduces by one the possible symbols that can follow any given one).

23.4.2 Diffusion

We now apply the formula (23.8) for a particular value of the spacing $w = 0.3$.

Together with estimates of the diffusion coefficient we may also provide estimates for the Lyapunov exponent (see sect. **??**). Moreover, since no trajectory escapes, the escape rate is zero, and the spectral determinant and the dynamical zeta function must satisfy the material flow conservation rule (19.11): the results for all these quantities are reported in table 23.2, where cells have been sampled with the variational method described in remark T.9.

LR: column 5 fixed by Lamberto

As mentioned above a lot of symbol sequences are pruned when the required finite horizon is achieved by making the spacing between disks small enough. So very poor convergence of cycle expansions has to be expected. With this in mind the numbers given in table 23.2 are in a reasonable accord with the probability conservation and offer a rather poor, but not unreasonable, estimate of the Lyapunov exponent. Nevertheless, the estimates of the diffusion constant up to the number of cycles employed so far appear to converge very slowly. They seem to be more sensitive to the bad shadowing than the Lyapunov exponent and the probability conservation. Of course, one should remember that the diffusion coefficient is a higher order moment of the generating function, hence it should be expected to be harder to get.

A way to circumvent the poorness of shadowing, due to severe and badly controllable pruning, is just going back to trace formulas (**??**)

$$D_{tr} = \frac{1}{4} \lim_{n\to\infty} \frac{\sum_{x\in Fix(n)} \hat{n}_x^2/|\Lambda_x|}{\sum_{x\in Fix(n)} T_x/|\Lambda_x|} \qquad (23.35)$$

For cycle length 9 ref. [23.2] reports $D_{tr} \simeq 0.240$, and for cycle length 10 $D_{tr} \simeq 0.2501$, which is not too far from the result of direct simulations (see

Figure 23.8: Finite order estimates for the diffusione coefficient from cycle expansions and trace formulas.

figure 23.8 tex fil is using too much memory, cannot latex book

figure 23.8). The apparent better performance of trace formulas over cycle expansions in this context is rather unexpected, and no strong theoretical clue is offered to justify this observation, but the very simple fact that trace formulas automatically include probability conservation, as the average is always computed by using a normalized measure. This fact suggests that the performance of cycle expansions for systems with strong pruning, might be improved by imposing by hand the condition of probability conservation at all orders of approximation.

⇑PRELIMINARY

Commentary

Remark 23.1 Lorentz gas. The original pinball model proposed by Lorentz [23.3] consisted of randomly, rather than regularly placed scatterers.

Remark 23.2 Who's dun it? Cycle expansions for the diffusion constant of a particle moving in a periodic array have been introduced independently by R. Artuso [23.4] (exact dynamical zeta function for 1-d chains of maps (23.8)), by W.N. Vance [23.5](the trace formula (23.35) for the Lorentz gas), and by P. Cvitanović, J.-P. Eckmann, and P. Gaspard [23.6] (the dynamical zeta function cycle expansion (23.8) applied to the Lorentz gas).

⇓PRELIMINARY
⇑PRELIMINARY

add Schreiber ref.

Remark 23.3 Lack of structural stability for D. Expressions like (23.20) may lead to an expectation that the diffusion coefficient (and thus transport properties) are smooth functions of the chaoticity of the system (parametrized, for example, by the Lyapunov exponent $\lambda = \ln \Lambda$). This turns out not to be true: D as a function of Λ is a fractal, nowhere differentiable curve shown in figure 23.5. The dependence of D on the map parameter Λ is rather unexpected - even though for larger Λ more points are mapped outside the unit cell in one iteration, the diffusion constant does not necessarily grow. The fractal dependence of diffusion constant on the map parameter is discussed in refs. [23.7, 23.8, 23.9]. Statistical mechanicians tend to believe that such complicated behavior is not to be expected in systems with very many degrees of freedom, as the addition to a large integer dimension of a number smaller than 1 should be as unnoticeable as a microscopic perturbation of a macroscopic quantity. No fractal-like behavior of the conductivity for the Lorentz gas has been detected so far [23.10].

Remark 23.4 Diffusion induced by 1-d maps. We refer the reader to refs. [23.11, 23.12] for early work on the deterministic diffusion induced by 1-dimenional maps. The sawtooth map (23.9) was introduced by Grossmann and Fujisaka [23.13] who derived the integer slope formulas (23.20) for the diffusion constant. The sawtooth map is also discussed in refs. [23.14].

length	# cycles	ζ(0,0)	λ
1	5	-1.216975	-
2	10	-0.024823	1.745407
3	32	-0.021694	1.719617
4	104	0.000329	1.743494
5	351	0.002527	1.760581
6	1243	0.000034	1.756546

Table 23.3: Fundamental domain, w=0.3 .

Jonqui"'ere function

Remark 23.5 Symmetry factorization in one dimension. In the $\beta = 0$ limit the dynamics (23.11) is symmetric under $x \to -x$, and the zeta functions factorize into products of zeta functions for the symmetric and antisymmetric subspaces, as described in sect. 22.1.2:

$$\frac{1}{\zeta(0,z)} = \frac{1}{\zeta_s(0,z)} \frac{1}{\zeta_a(0,z)} , \qquad \frac{\partial}{\partial z}\frac{1}{\zeta} = \frac{1}{\zeta_s}\frac{\partial}{\partial z}\frac{1}{\zeta_a} + \frac{1}{\zeta_a}\frac{\partial}{\partial z}\frac{1}{\zeta_s} . \tag{23.36}$$

The leading (material flow conserving) eigenvalue $z = 1$ belongs to the symmetric subspace $1/\zeta_s(0,1) = 0$, so the derivatives (23.15) also depend only on the symmetric subspace:

$$\langle n \rangle_\zeta = z\frac{\partial}{\partial z}\frac{1}{\zeta(0,z)}\bigg|_{z=1} = \frac{1}{\zeta_a(0,z)}\, z\frac{\partial}{\partial z}\, \frac{1}{\zeta_s(0,z)}\bigg|_{z=1} . \tag{23.37}$$

Implementing the symmetry factorization is convenient, but not essential, at this level of computation.

Remark 23.6 Lorentz gas in the fundamental domain. The vector valued nature of the generating function (23.3) in the case under consideration makes it difficult to perform a calculation of the diffusion constant within the fundamental domain. Yet we point out that, at least as regards scalar quantities, the full reduction to $\tilde{\mathcal{M}}$ leads to better estimates. A proper symbolic dynamics in the fundamental domain has been introduced in ref. [23.15], numerical estimates for scalar quantities are reported in table 23.3, taken from ref. [23.16].

In order to perform the full reduction for diffusion one should express the dynamical zeta function (23.7) in terms of the prime cycles of the fundamental domain $\tilde{\mathcal{M}}$ of the lattice (see figure 23.2) rather than those of the elementary (Wigner-Seitz) cell $\mathcal{M}$. This problem is complicated by the breaking of the rotational symmetry by the auxilliary vector β, or, in other words, the non-commutativity of translations and rotations: see ref. [23.6].

Remark 23.7 Anomalous diffusion. Anomalous diffusion for 1-d intermittent maps was studied in the continuous time random walk approach in refs. [21.10, 21.11]. The first approach within the framework of cycle expansions (based on truncated dynamical zeta functions) was proposed in ref. [21.12]. Our treatment follows methods introduced in ref. [21.13], applied there to investigate the behavior of the Lorentz gas with unbounded horizon.

stosszahlansatz
Boltzmann!equation

Remark 23.8 Jonquière functions. In statistical mechanics Jonquière functions

$$J(z,s) = \sum_{k=1}^{\infty} z^k/k^s \tag{23.38}$$

appear in the theory of free Bose-Einstein gas, see refs. [21.21, 21.22].

Résumé

Boltzmann refs.

The classical Boltzmann equation for evolution of 1-particle density is based on *stosszahlansatz*, neglect of particle correlations prior to, or after a 2-particle collision. It is a very good approximate description of dilute gas dynamics, but a difficult starting point for inclusion of systematic corrections. In the theory developed here, no correlations are neglected - they are all included in the cycle averaging formula such as the cycle expansion for the diffusion constant

$$D = \frac{1}{2d}\frac{1}{\langle T\rangle_\zeta}\sum{}'(-1)^{k+1}\frac{(\hat{n}_p+\cdots)}{|\Lambda_p\cdots|}\frac{(\hat{n}_{p_1}+\cdots+\hat{n}_{p_k})^2}{|\Lambda_{p_1}\cdots\Lambda_{p_k}|}\,.$$

Such formulas are *exact*; the issue in their applications is what are the most effective schemes of estimating the infinite cycle sums required for their evaluation. Unlike most statistical mechanics, here there are no phenomenological macroscopic parameters; quantities such as transport coefficients are calculable to any desired accuracy from the microscopic dynamics.

Though superficially indistinguishable from the probabilistic random walk diffusion, deterministic diffusion is quite recognizable, at least in low dimensional settings, through fractal dependence of the diffusion constant on the system parameters, and through non-Gaussion relaxation to equilibrium (non-vanishing Burnett coefficients).

For systems of a few degrees of freedom these results are on rigorous footing, but there are indications that they capture the essential dynamics of systems of many degrees of freedom as well.

Actual evaluation of transport coefficients is a test of the techniques developped above in physical settings. In cases of severe pruning the trace formulas and ergodic sampling of dominant cycles might be more effective strategy than the cycle expansions of dynamical zeta functions and systematic enumeration of all cycles.

References

[23.1] J. Machta and R. Zwanzig, *Phys. Rev. Lett.* **50**, 1959 (1983).

[23.2] G.P. Morriss and L. Rondoni, *J. Stat. Phys.* **75**, 553 (1994).

[23.3] H.A. Lorentz, *Proc. Amst. Acad.* **7**, 438 (1905).

[23.4] R. Artuso, *Phys. Lett.* **A 160**, 528 (1991).

[23.5] W.N. Vance, *Phys. Rev. Lett.* **96**, 1356 (1992).

[23.6] P. Cvitanović, J.-P. Eckmann, and P. Gaspard, *Chaos, Solitons and Fractals* **6**, 113 (1995).

[23.7] R. Klages, *Deterministic diffusion in one-dimensional chaotic dynamical systems* (Wissenschaft & Technik-Verlag, Berlin, 1996); `www.mpipks-dresden.mpg.de/ rklages/publ/phd.html`.

[23.8] R. Klages and J.R. Dorfman, *Phys. Rev. Lett.* **74**, 387 (1995); *Phys. Rev. E* **59**, 5361 (1999).

[23.9] R. Klages and J.R. Dorfman, "Dynamical crossover in deterministic diffusion", *Phys. Rev.* **E 55**, R1247 (1997).

[23.10] J. Lloyd, M. Niemeyer, L. Rondoni and G.P. Morriss, *CHAOS* **5**, 536 (1995).

[23.11] T. Geisel and J. Nierwetberg, *Phys. Rev. Lett.* **48**, 7 (1982).

[23.12] M. Schell, S. Fraser and R. Kapral, *Phys. Rev.* **A 26**, 504 (1982).

[23.13] S. Grossmann, H. Fujisaka, Phys. Rev. **A 26**, 1179 (1982); H. Fujisaka and S. Grossmann, Z. Phys. **B 48**, 261 (1982).

[23.14] P. Gaspard and F. Baras, in M. Mareschal and B.L. Holian, eds., *Microscopic simulations of Complex Hydrodynamic Phenomena* (Plenum, NY 1992).

[23.15] F. Christiansen, Master's Thesis, Univ. of Copenhagen (June 1989).

[23.16] P. Cvitanović, P. Gaspard, and T. Schreiber, "Investigation of the Lorentz Gas in terms of periodic orbits", *CHAOS* **2**, 85 (1992).

[23.17] S. Grossmann and S. Thomae, *Phys. Lett.*__A 97__, 263 (1983).

[23.18] R. Artuso, G. Casati and R. Lombardi, *Physica* **A 205**, 412 (1994).